In: Wang, X.; Sauter, U.H.; Ross, R.J., eds. 2019. Proceedings: 21st International Nondestructive Testing and Evaluation of Wood Symposium. General Technical Report FPL-GTR-272. Madison, WI: U.S. Department of Agriculture, Forest Service, Forest Products Laboratory. pp 502-510.

Using Ground Penetrating Radar to Classify Features within Structural Timbers

Xi Wu
School of IoT Engineering, Jiangnan University, Wuxi, Jiangsu, China, 335722038@qq.com

Christopher Adam Senalik
USDA Forest Service, Forest Products Laboratory, Madison, Wisconsin, USA, christopher.a.senalik@usda.gov

James Wacker
USDA Forest Service, Forest Products Laboratory, Madison, Wisconsin, USA, james.p.wacker@usda.gov

Xiping Wang
USDA Forest Service, Forest Products Laboratory, Madison, Wisconsin, USA, xiping.wang@usda.gov

Guanghui Li
School of IoT Engineering, Jiangnan University, Wuxi, Jiangsu, China, ghli@jiangnan.edu.cn

Abstract

Recent developments in image processing play a significant role in identifying and classifying features on ground penetrating radar (GPR) radargrams. Two groups of timber specimens were examined in this study. The first group comprised laboratory prepared Douglas-fir (*Pseudotsuga menziesii*) timber sections with inserts of known internal characteristics. The second group comprised timber girders salvaged from timber bridges on historic Route 66 that had been exposed to weather for more than 80 years. A subsurface interface radar system with a 2-GHz palm antenna was used to scan these two groups of specimens. GPR sensed differences in dielectric constants along the scan path caused by the presence of water, metal, or air within the wood. This study focused on two procedures: feature identification and classification. Image processing was used to identify the presence of defect features, which was then classified based upon machine learning. GPR radargrams proved to be an excellent tool to detect and define characteristics within structural timbers.

Keywords: ground penetrating radar, timber, metal, moisture content, image processing, feature classification

Introduction

Nondestructive testing (NDT) techniques are needed by engineers and inspection professionals to evaluate the internal condition of wood structures. This study used ground penetrating radar (GPR), a GSSI (Nashua, New Hampshire, USA) Subsurface Interface Radar (SIR) 4000 with a 2-GHz palm antenna, to scan two groups of timber beam specimens. Results of the radar wave tests on controlled specimens were calibrated and used to develop recognition methods on beams that had served out their lives in an actual bridge structure.

GPR technology has been widely used for detecting buried objects of various materials such as sand, timber, concrete, etc. It has been clearly illustrated that GPR can detect anomalous electromagnetic responses associated with a variety of significant physical conditions (Pettinelli et al. 2009). GPR uses an antenna to generate short bursts of electromagnetic energy in solid materials.Waveforms are transmitted into the structure using an antenna positioned at the surface. A portion of the wave is reflected, refracted, and/or diffracted when encounterring the boundary of objects with different dielectric constant and then is received by the antenna. Schad et al. (1996) investigated three nondestructive evaluation techniques for detecting internal wood defects. Both sound wave transmission and impulse radar were able to detect large voids and areas of degradation. The use of radar requires an experienced operator because of the difficulty of interpreting the data. Brashaw (2014) researched the signal analyzing of the radar data in both the longitudinal direction (antenna front to back) and the transverse direction (antenna side to side). This research was designed to be an early assessment of the potential for using GPR to identify known defects in longitudinal timber bridge decks and slab spans. The results of their experiments provide ideas for future study in GPR. The incident wave propagates through the material and partially reflects at interfaces presenting a dielectric contrast (Benson 1995, Rodríguez-Abad et al. 2011). The electromagnetic response of all the reflected waves could be processed and analyzed to estimate propagation velocities or depth of objects.

The wave forms visible in one-dimensional data (A-scan) and two-dimensional radargrams (B-scan) contain information about internal characteristics of the analyzed specimen. Unfortunately, the wave forms also contain a variety of complex interference waves, increasing the difficulty of feature identification.

In order to obtain high quality signals, the noise level must be suppressed. One method of signal denoising is the empirical mode decomposition (EMD). EMD was proposed by Huang et al. (1998). The EMD method has had significant impact and is widely used in a broad variety of time-frequency analysis applications (Dragomiretskiy and Zosso 2014) as well as signal processing. It has the advantage of determining the amplitude of the signal and adaptively decomposing the signal into a stationary signal. The finite number of IMF (Intrinsic Mode Function) components decomposed represents the physical characteristic information of the signal. Battista et al. (2007) used EMD to remove cable strum noise from seismic data. Narayanan et al. (2010) used the EMD method to mitigate both coherent and random noise in wall radar human detection.

After denoising the signal data, regions containing defects must be located. Dynamic time warping (DTW) is a way to measure the similarity of two time series of different lengths. DTW is a typical optimization problem; it uses the time-warping function to demonstrate the time corresponding relation between a test template and reference template. Warping one (or both) of the sequences in the timeline can achieve better alignment. Then, the time-warping function corresponding to the minimum cumulative distance between the two templates can be calculated.

DTW is a commonly used technique to accomplish this task. This method plays an important role in speech recognition and machine learning convenience. Jazayeri et al. (2018) proposed a cutting-edge expert system by setting a threshold on DTW values and monitoring them online. A significant deviation of the DTW values from the reference signal is detected prior to reaching an object.

Feature extraction plays an important role in target recognition and classification of GPR signals. Selecting appropriate features can not only reduce the computational complexity of GPR echo signal analysis but also improve target detection and classified performance. Feature extraction after denoising and similarity analyzing was conducted based on the discrete wavelet transformation (DWT). Baili et al. (2009) presented the use of DWT to denoise the GPR signals. Various other wavelets were used in this study to denoise experimental GPR signals collected from flexible pavements. Bruce et al. (2002) used

DWT for hyperspectral feature extraction and signature classification. Wavelet-based feature extraction, specifically the use of subsets of DWT coefficients, was developed and applied to two precision agricultural applications. Their experimental results show a superior performance of the proposed wavelet-based features for the hyperspectral classification compared with more conventional methods.

The main purpose of this paper is to recognize and locate the defects. Some of the many methods used for GPR data were used on our data. A list of processing steps was used to analyze the A-scan and B-scan data.

Materials and Methods

Materials

There are two groups of data obtained from Douglas-fir (*Pseudotsuga menziesii*). The first group was based on a timber bridge project. A unique set of aged highway timber bridges are located along a portion of the historic U.S. Route 66 in southern California. This stretch of historic Route 66 in the Mojave Desert is currently the focus of extensive efforts by the County of San Bernardino to preserve its iconic legacy and protect its key cultural and historical resources, which include the timber bridge structures (Wacker et al. 2017). A total of 18 timbers beams were used in this study. Prior to testing, the beams were brought to a moisture content (MC) equilibrium of 10% in a temperature- and humidity-controlled room. The second group was five core samples at varying moisture contents and two samples with metal bars (nails and screws) inserted parallel to the length of the cores. The scanning process of bridge timbers is shown in Figure 1. The diameter of the bars were 1.6, 4.8, and 7.9 mm (1/16, 3/16, and 5/16 in.) as shown in Figure 2a. Placement of the core samples into the cavity of timber sections is shown in Figure 2b. The GPR antenna was placed on top of the timber section, and the scan was performed down through the inserted core.

The majority of the defects in the Route 66 bridge timbers are the metal bars that were used to strengthen and secure the bridge. The presence of the metal bars commonly resulted in holes and cracks throughout the timbers. Figure 3 shows the defect statistics of the 18 timbers, which were calculated based on the defect mapping documents and camera pictures.

Methods

The object detection algorithm can be divided into five steps: (1) using EMD to decompose A-scan data into IMFs; (2) calculating the similarities using DTW based on IMF1; (3) estimating the position of defects by comparing the similarities of data from each scan; (4) selecting some windows on B-scan including defects as a portion of the database, according to the location of each defect and the analyzed data; and (5) extracting the features of each region. A flowchart of this proposed strategy is given in Figure 4.

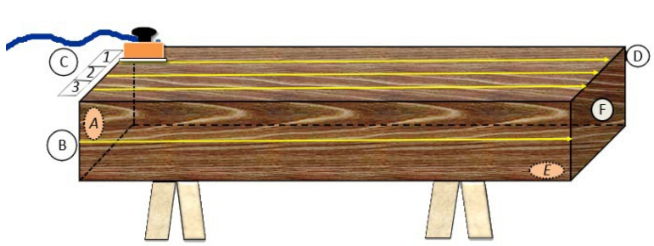

Figure 1—Display of the scanning process.

(a) (b)

Figure 2—(a) The core samples with inserted metal nails and bars of different sizes; (b) the testing environment of core samples.

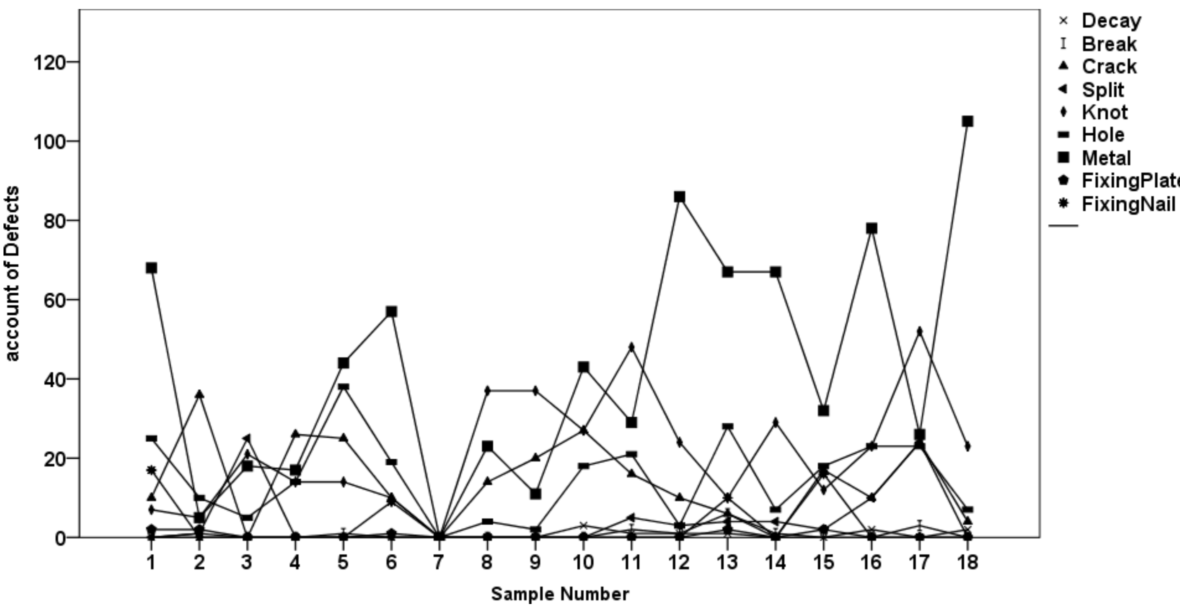

Figure 3—Defect accounts of 18 timbers tested in laboratory.

To ensure the accuracy of processing, we analyzed the raw data (.dzt format files) under the MATLAB environment. Detailed procedures are subsequently shown:

(1) Find the maximum values (Rmax) and minimum values (Rmin) of the raw signal $R(n)$. From these extreme points, the upper and lower curves are called $R\max(n)$ and $R\min(n)$, and the average envelope $\mathrm{Avg}(n)$ between these two envelopes could be calculated by Equation (1):

$$\mathrm{Avg}(n) = \frac{R\max(n) + R\min(n)}{2} \quad (1)$$

(2) The variable $Rl(n) = R(n) - \mathrm{Avg}(n)$ sets the reference function that satisfies the IMF condition as $c(n)$. Then, repeat Steps (1) and (2) until the first IMF is obtained.

(3) The residual component $Rr(n)$ could be calculated by Equation (2):

$$Rr(n) = R(n) - C_1(n) \tag{2}$$

(4) Using $Rr(n)$ as the new signal needing to be processed, repeat the previous steps until all IMF components are obtained. The original A-scan data were finally decomposed into

$$Rl(n) = \sum_{i=1}^{m} C_i(n) + Rr_m(n)b \tag{3}$$

(5) Choose five column vectors of the first IMF, which has almost no defects. Then the average (t (t_1, t_2, t_3, ..., t_n)) of these five vectors represents the reference signal. The test vector (r (r_1, r_2, r_3, ..., r_n)) is each signal data point of IMF. The DTW process starts by constructing an $n \times m$ matrix in which the element of the (i, j)th component corresponds to the following squared Euclidian distance:

$$\mathrm{dist}(t_i, r_i) = (t_i - r_i)^2 \tag{4}$$

(6) Retrieve an optimal path by using an iterative method through the $n \times m$ matrix that minimizes the total cumulative distance between the two signals:

$$D(t, r) = \sqrt{\sum_{m=1}^{m} \mathrm{dist}_m} \tag{5}$$

where dist_m is the mth element of the warping path.

Each defect was located by targeting the peak point of each dist(m). The Euclidean distance matrix of the column vector in which the peak is located represents the similarity for two equally sized waves. The maximum in the diagonal direction of the D matrix relatively represents the peak of the hyperbolic reflection wave. Locating these points is equivalent to find the area of the defect. The next step is to extract more features from B-scan images to get more comprehensive information for the defect region.

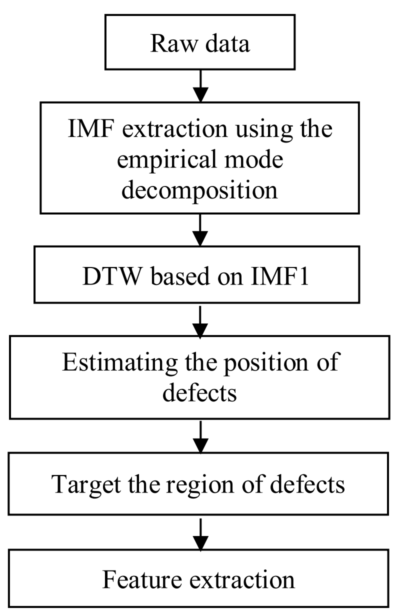

Figure 4— A flowchart of data processing of proposed detection algorithm.

Results

Five core samples with 68.26-mm- (2-11/16-in.-) and 133.35-mm- (5-1/4-in.-) diameter were soaked for several hours. After soaking, they were weighed and then scanned as shown in Figure 2b. After scanning, the cores were returned to the water bath to continue soaking. After the tests were completed, the cores were oven-dried to calculate the exact MC. Five soak times were chosen (2, 7.5, 24, 55.5, and 120 h) based on the expert's advice. The weights at different times are shown in Table 1. It is obvious that the MC was increasing with a relatively stable state, about 7% incremental value.

Table 1—Moisture content of the soaked core samples by hours of soaking.

Sample	Moisture content (%)					
	0 h	2 h	7.5 h	24 h	55.5 h	120 h
1	6	14	20	27	35	46
2	6	14	19	23	36	47
3	6	15	21	28	35	45
4	6	14	18	25	31	39
5	6	14	19	26	33	42

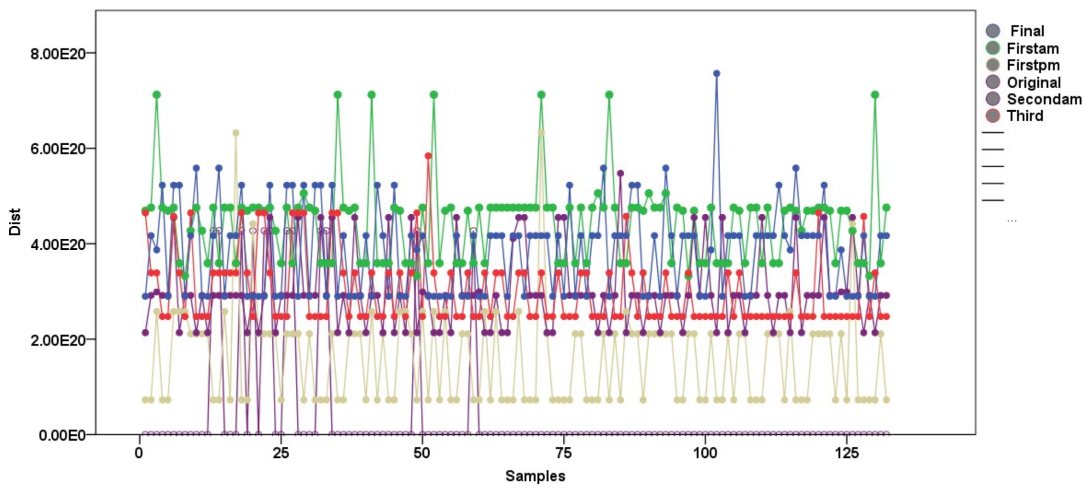

(a)

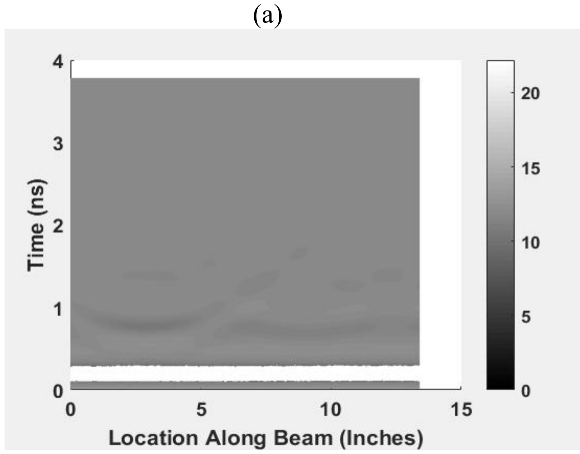

(b)

Figure 5—(a) The DTW data of the No. 6 core sample; (b) the radargrams when the No. 6 core sample was inserted (1 in. = 25.4 mm).

Figure 5a displays the similarities of the No. 3 sample with different MC. It can be seen that the fluctuant trend of the Dist data were different in Figure 5a. The center position of the inserted core sample was at 149.2 mm (5-7/8 in.), and the center of an adjacent smaller hole was at 298.5 mm (11-3/4 in). Figure 5b show the B-scan radargram (soaked for 120 h) generated from MATLAB. The hyperbolas indicating the presence of the core sample and the hole affects each other; they overlap in the middle region between core sample and hole. To facilitate the experiments, without damaging the inserted samples and the timber section, the diameter of the core sample is usually smaller than the size of the insert hole (shown in Fig. 2b). Gaps between the outside boundary of the sample and the upper surface of the hole are visible. When MC exceeded 35%, the upper area of the hyperbola had some new reflected waves, which were probably caused by the gaps. The gap also provides an explanation to the suddenly higher DTW data in the core sample region.

The two core samples had different sizes of nails or bars. There were three sizes of metal nails tested. The diameter of the two sizes of metal bars were 9.525 mm (3/8 in.) and 12.7 mm (1/12 in.). As shown in Figure 6a, the first five scan samples were chosen to calculate the average data as the base vector. The highest DTW value near 50.8 mm (2 in.) indicates the center of the bars. Because of the principle of radar collecting the reflections, the entire extended surface of the hyperbola waves almost covered the whole width (Fig. 6b). Apparently, the diffraction wave of the core samples was combined with the hole reflection wave. The relative higher peaks in Figure 6a illustrated the overlap reflected waves between core sample and hole or the gap and the core sample in the whole section.

The data group from the Route 66 wood timbers included defect indications from many metal bars (7.9 mm (5/16 in.)), holes, and knots. For the timber beams, the data were collected on scanning lines that covered much more metal material on timbers. These were analyzed using EMD and DTW. As shown in Figure 7a, each peak point represents metal bars. Besides the points with extremely high values, the other apparently visible and highlighted hyperbolas (Fig. 7b) correspond to the relatively smaller and slightly prominent peak points in Figure 7a. These DTW values were similar and in a stable extent. However, the blurred hyperbola (Fig. 7b) between 2.0 and 2.5 m (80 and 100 in.) was found to be a hole after consulting pictures of the timber. It has a smaller DTW value than those of the metal bars.

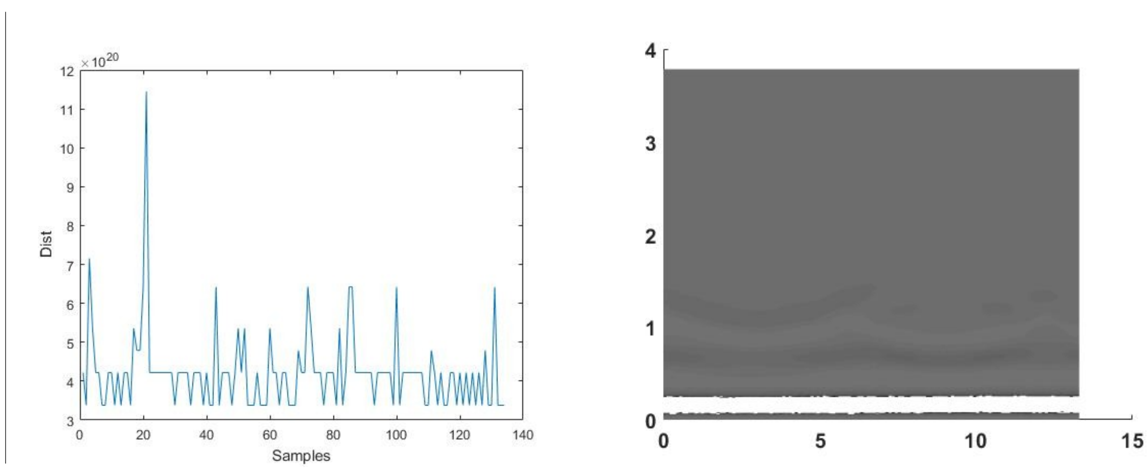

(a) (b)

Figure 6—(a) The DTW data calculated from the core sample that was inserted with a 12.7-mm (1/12-in.) metal bar; (b) the radargrams of this core sample.

The sudden extremely high DTW value usually appeared in the areas that include at least two hyperbolas. These hyperbolas were close to each other, and in some cases, overlapped within the adjacent regions. The timbers were placed on two wood supports during testing. Each timber was 101.6 mm (4 in.) thick. This situation commonly produces noise in the raw data. Even after the denoising process on the A-scan data, the noise in the reflected waves cannot be completely removed. In total, 737 peak points were found based on the data of Figure 7a. These peaks represent the metal bars, holes, knots, etc. Then the range of DWT values corresponding to different defects should be separately recorded. The approximate location of defects on the radargrams is converted from the position of the peak on a single channel signal. According to the locations, extracting an area with 70 * 270 pixels around the points. After that, features could be extracted on the radargrams with different types of defects. All the peaks seen in Figure 7a correspond to nails. The values for knots are relatively small and cannot be seen in the figure.

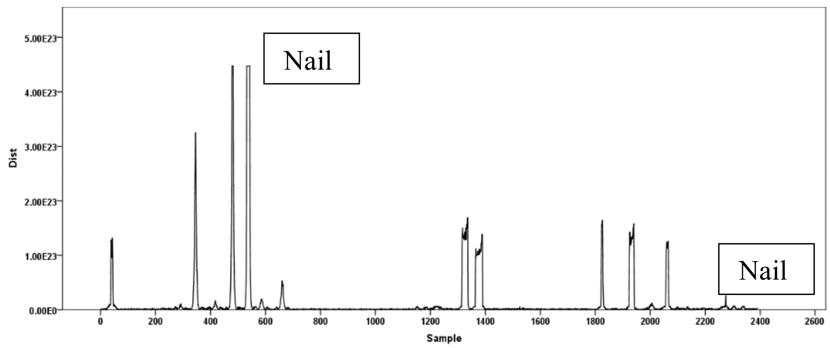

(a)

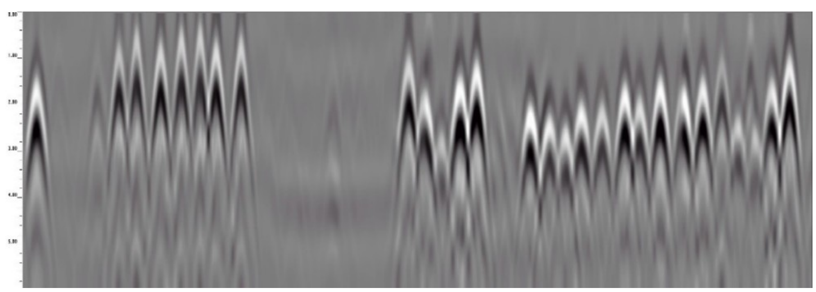

(b)

Figure 7—(a) The line chart of DTW values; (b) the radargrams generated from RADAN 7.

Conclusions and Discussion

This study demonstrated the effectiveness of using a combination processing method to locate and define the defects of wood timbers. The Route 66 bridge timbers are complex, real-world specimens. The timbers are inhomogeneous, containing cracks, splits, holes, metal bars, and naturally occuring decay from years of exposure and use, all of which increases the complexity of the analysis process. Some detection methods were not capable of identifying these conditions, such as some image segmentation methods to target the hyperbola regions. We used a list of processing steps that could locate the defects, including some defects that are invisible in the radargrams. EMD and DTW are efficient for the GPR data of wood timbers. These results display the ability to illustrate some invisible feature information of signals after comparing with radargrams. At the same time, these works play an important role before extracting the features of defect regions on the radargrams. Although EMD and DTW have shown positive results in locating and classifying defects, some vague regions still exist. In the future, there is a need to further improve these methods and add signal gain processing steps to enhance the brightness and contrast of radargrams for easy observation and comparison. Obtaining additional specimens with reduced complexity would aid in analysis.

Acknowledgments

This paper describes a study conducted by the USDA Forest Service, Forest Products Laboratory, in cooperation with the County of San Bernardino (California) and Biggs Cardosa Associates, Inc. Ms. Xi Wu's participation in this project was supported by the China Scholarship Council.

References

Baili, J.; Lahouar, S.; Hergli, M.; Al-Qadi, I.L.; Besbes, K. 2009. GPR signal de-noising by discrete wavelet transform. NDT & E International. 42(8): 696-703.

Battista, B.M.; Knapp, C.; McGee, T.; Goebel, V. 2007. Application of the empirical mode decomposition and Hilbert–Huang transform to seismic reflection data. Geophysics. 72(2): 29-37.

Benson, A.K. 1995. Applications of ground penetrating radar in assessing some geological hazards: examples of groundwater contamination, faults, cavities. Journal of Applied Geophysics. 33: 177-193.

Brashaw, B.K. 2014. Inspection of timber bridge longitudinal decks with ground penetrating radar. Ph.D. Dissertation. Mississippi State University, ProQuest Dissertations Publishing. 3665457.

Bruce, L.M.; Koger, C.H.; Li, J. 2002. Dimensionality reduction of hyperspectral data using discrete wavelet transform feature extraction. In: IEEE Transactions on Geoscience and Remote Sensing. 40(10): 2331-2338.

Dragomiretskiy, K.; Zosso, D. 2014. Variational mode decomposition. In: IEEE Transactions on Signal Processing. 62(3): 531-544.

Huang, N.E.; Shen, Z.; Long, S.R.; [and others]. 1998 The empirical mode decomposition and the Hilbert spectrum for nonlinear and non-stationary time series analysis. Proceedings of the Royal Society of London A: Mathematical, Physical and Engineering Sciences. 454: 903-995.

Jazayeri, S.; Saghafi, A.; Esmaeili, S.; Tsokos, C. 2018. Automatic object detection using dynamic time warping on ground penetrating radar signals. Expert Systems with Applications. 122: 102-107.

Narayanan, R.M.; Shastry, M.C.; Chen, P.-H.; Levi, M. 2010. Through -the-wall detection of stationary human targets using Doppler radar. Progress in Electromagnetics Research B. 20: 147-166.

Pettinelli, E.; Matteo, A.D.; Mattei, E.; Crocco, L.; [and others]. 2009. GPR response from buried pipes: measurement on field site and tomographic reconstructions. IEEE Transactions on Geoscience and Remote Sensing. 47(8): 2639-2645.

Rodríguez-Abad, I.; Martínez-Sala, R.; Capuz, R.; Díez, R.; García, F. 2011. Assessment of the variation of the moisture content in the *Pinus pinaster* Ait. using the non destructive GPR technique. Materiales De Construccion. 61(301): 143-156.

Schad, K.C.; Schmold, D.L.; Ross, R.J. 1996. Nondestructive methods for detecting defects in softwood logs. Research Paper FPL-RP-546. Madison, WI: U.S. Department of Agriculture, Forest Service, Forest Products Laboratory.

Wacker J, Mikhail M, Dizon G (2017) Evaluation of Bridge Components Salvaged from Historic Route 66 in California. Research in Progress RIP-4719-038. USDA Forest Service, Forest Products Laboratory, Madison, WI. https://www.fpl.fs.fed.us/documnts/rips/fplrip-4719-038-Wacker-Mikhail-Dizon.pdf.